Research Article

Jianbo Liao*, Aihua Xi, Sujuan Liang, Xinping Zhou, Zhiyong Li, Jun Di, Wenting Zhang, Rong Wanyan, and Pinghui Yu

Genetic mechanisms of deep-water massive sandstones in continental lake basins and their significance in micro–nano reservoir storage systems: A case study of the Yanchang formation in the Ordos Basin

https://doi.org/10.1515/ntrev-2020-0040
received January 20, 2020; accepted April 24, 2020

Abstract: Based on field geological surveys of two deep-water sedimentary outcrops in the Yanchang formation of the Ordos Basin, X-ray diffraction analysis, elemental geochemical analysis, and polarizing microscope observations were conducted to investigate the causes of various sedimentary structures inside the massive sand bodies from deep-water debris flow. A genesis model of deep-water debris-flow sandstone is established: during the handling of the mass transport complexes in the basin slope, the soft sandy sedimentary layer with relatively strong shear resistance tears the soft muddy sedimentary layer with weak shear resistance and pulls various clumps inside the muddy layer. Finally, debris-flow massive sandstones with rich sedimentary structures are formed. Through argon ion polishing and field emission scanning electron microscopy, the debris-flow sandstones mainly develop micron-scale pores, and the pore radius is mainly distributed in the range of 1–8 μm. The sedimentary rocks from the semi-deep lake to deep lake facies only have a small number of nano-scale pores, and the pore radius is distributed between 20 and 120 nm.

Keywords: FESEM, geochemistry, micro-nano, nanopore, Ordos Basin, sedimentary structure, storage system, Yanchang formation

1 Introduction

Genetic mechanisms of deep-water sandstones have attracted considerable attention in both the petroleum industry and sedimentology research [1–3]. Deep-water gravity flow deposit processes are extremely complex, and the evolution of their internal fluid properties is variable [4]. Current studies can only infer sedimentary genesis but cannot determine the overall sedimentary processes and their evolution [5–7], which could limit our understanding of the genetic mechanisms and distribution of deep-water sediments. Deep-water gravity flow deposits include rockslides, slumps, liquefied sediment flows, sandy debris flows, muddy debris flows, and turbidites [8,9]. Of these deposits, debris-flow sandstones have good reservoir properties such as great thickness and wide distribution that have gradually attracted more attention [2,6,10–12].

According to the sandy debris flow identification basis proposed by Shanmugam [13], floating mudstone clasts are important sedimentary structures that develop within massive sandstones. However, for the origin and genesis of floating mudstone clasts, previous studies including Shanmugam's own research mostly focused on the observation and description of sedimentary phenomena. There are mainly three kinds of understanding based on speculation. One is that during the process of sandy slump and muddy debris flow formation, debris-flow mudstone in the shallow water area was drawn into the overlying sandy sediments [14]. Another type is believed to be eroded by the early

* **Corresponding author: Jianbo Liao,** School of Geoscience and Technology, Southwest Petroleum University, Chengdu, 610500, ChinaResearch Institute of Petroleum Exploration and Development Northwest Branch, Lanzhou, 730020, China; Key Laboratory of Reservoir Description, CNPC, Lanzhou, 730020, China, e-mail: liao_jb@petrochina.com.cn
Aihua Xi: School of Geoscience and Technology, Southwest Petroleum University, Chengdu, 610500, China
Sujuan Liang, Jun Di, Wenting Zhang, Rong Wanyan, Pinghui Yu: Research Institute of Petroleum Exploration and Development Northwest Branch, Lanzhou, 730020, China
Xinping Zhou: Exploralion & Development, PetroChina Changqing Oil field Company, Xi'an, 710018, China
Zhiyong Li: Research Institute of Petroleum Exploration and Development Northwest Branch, Lanzhou, 730020, China; Key Laboratory of Reservoir Description, CNPC, Lanzhou, 730020, China

turbidity on the underlying bed of the underlying lake, engulfing mudstone debris, and subsequently undergoing fluid conversion, thereby forming a sandy debris flow with mudstone tearing debris [15–19]. Some other scholars believe that due to turbidity or storms, the underlying sediments are strongly eroded, and the underlying unconsolidated or weakly consolidated sediments are agitated to form agitated layers of sand and mud [20,21]. The above controversy stems from the lack of targeted research on debris-flow sandstones, especially the lack of reliable experimental data. In order to solve the problems, the author carried out field geological surveys of two typical deep-water sedimentary outcrops in the Yanchang formation in the southern Ordos Basin. The internal sedimentary structures such as mudstone clasts, clumps, and "mud-coated intraclasts" in debris-flow sandstone were systematically investigated. Samples were collected and qualitatively analyzed based on experimental data such as X-ray diffraction analysis, trace element geochemical analysis, and polarizing microscope identification. Based on the experimental data, the deep-water mass transport deposits were accurately clarified. Sources and origins of inclusions such as mudstone clasts, clumps in sandstone, and a deterministic mechanism model have been established. Nanotechnology has achieved good application effect in oil and gas industries [22]; in this study, argon ion polishing and field emission scanning electron microscopy (FESEM) were used to analyze the pore development characteristics of debris-flow fine sandstones and other types of rocks in the deep-water sedimentary system. The deep-water "sweet spots" reservoirs were identified, and the pore radius scale range of micro–nano reservoir storage systems was obtained. The above research has important theoretical and practical significance for oil and gas exploration in deep-water micro–nano reservoir storage systems in continental lake basins.

2 Geologic setting

The Ordos Basin is a craton basin in central and northern China (Figure 1a). The area of the basin is about 25×10^4 km^2. The basin can be further divided into six first-order tectonic units: the Yimeng uplift, the western margin thrust belt, the Tianhuan depression, the Yishan slope, the Jinxi fold belt, and the Weibei uplift (Figure 1b). The Upper Triassic Yanchang formation is its main oil-bearing strata. The predecessors divided the Yanchang formation from top to bottom into ten oil-bearing formations [23]. Among them, Chang 10–Chang 8 is the initial stage of the lake basin development, Chang 7 is the peak expansion period of the lake basin, and Chang 6 is the large-scale constructive delta pre-filling period [24–26]. A delta deposition system in a large area of the lake basin is developed in the Chang 7–Chang 6_3 period. The semi-deep lake-deep lake sediments were widely developed along the center of the lake basin [27,28] (Figure 1b). In recent years, nearly one billion tons of reserves have been discovered for exploration in this area. The main oil-bearing sand bodies are deep-water massive sandstones [29–31]. It is of great theoretical and practical significance to study the source and genesis of the sedimentary structure in the sandstone.

In this study, two sections of the Shanshui River (Xunyi County) and Yaoqu (Tongchuan County) were selected for research in the Weibei uplift belt in the southern Ordos Basin (Figure 1b). Among them, the Chang 7 section of the Shanshuihe section is exposed 3 km northeast of Xunyi County. The lithology is composed of multiple sets of gray-black mud shale and gray-green block fine sandstone, thin layer of fine sandstone, and dark gray silty mudstone (Figure 2a). The Chang 7 section of the Yaoqu section is exposed in Yaoqu Town, Tongchuan County. The sandstone layer in the profile gradually becomes thinner upward, and the mudstone increases, reflecting a set of decumbent sediments that the lake water gradually changes from shallow to deep. The lithological combination consists of multiple sets of yellow-gray blocky fine sandstones, thin-layered fine-grained sandstones, and dark gray silty mudstones (Figure 2b).

Previous studies demonstrated that the thick massive sandstones in the two sections represent semi-deep to deep debris-flow deposition [30,31]. The massive sandstones (0.5 to 3 m thick) are associated with dark gray mudstone (debris-flow mudstone), thin silty sandstone, and gray-black laminated shale. The debris-flow sandstones have abundant internal depositional structures and contain floating mudstone clasts, clumps, and mud-coated intraclasts [32]. The mudstone clasts are mostly sharp-edged, elongated, and aligned in their long direction (Figure 3a and b). The clumps are mostly yellow-brown and spindle-shaped (Figure 3e). The mud-coated intraclasts have a two-layered structure composed of a spindle or oval-shaped block and a muddy or silty mud coating less than 3 cm thick (Figure 3a and k).

3 Materials and methods

We systematically sampled floating mudstone clasts, clumps, and mud-coated intraclasts within the debris-flow

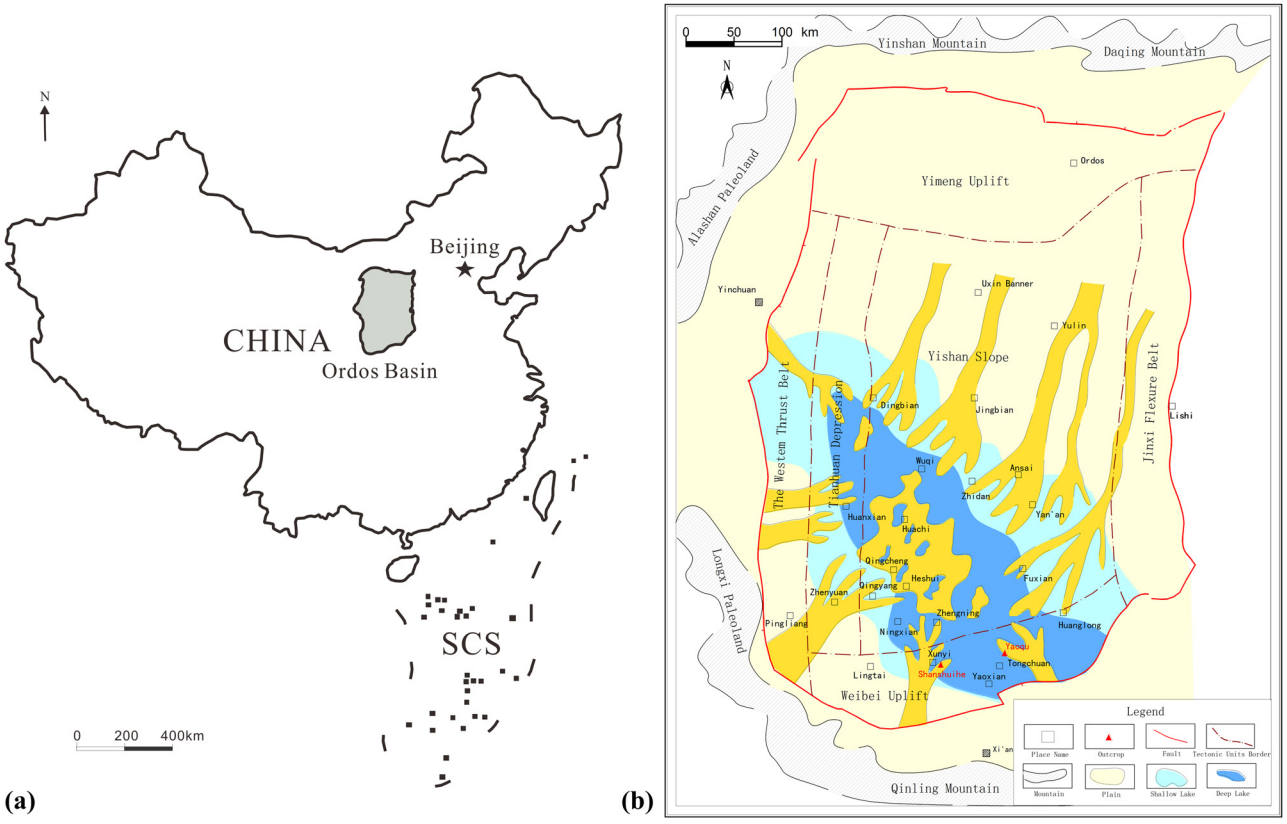

Figure 1: (a) Location of the Ordos Basin, central China. (b) Ordos Basin tectonic unit and extended lake-delta system map.

sandstones as well as mudstones and clumps within the associated debris-flow mudstones and laminated mudstones. Samples were obtained from both outcrop sections (Yaoqu and Shanshuihe), which showed fresh cutting surfaces due to natural collapse and road construction, and had not been affected by alteration and weathering, indicating that subsequent analytical results were reliable.

Trace element geochemistry, X-ray powder diffraction (XRD), and thin section analyses were carried out to describe the depositional environment, bulk composition, and lithological characteristics of the collected samples. The relationship among the internal sedimentary structures of the massive sandstones, associated debris-flow mudstones, and laminated mudstones can be determined to reveal the genetic mechanisms further.

Trace element geochemical analyses were carried out at the State Key Laboratory of Marine Geology (Tongji University) using an inductively coupled plasma mass spectrometer (Thermo Fisher VG-X7). In the test, a mixed solution of nitric acid (HNO_3) and hydrofluoric acid was used to remove the siliceous and carbonate minerals in the rock sample. During the measurement runs, 1 ppb of rhenium (Re) and rhodium (Rh) were used as internal standards to monitor the instrument stability dynamically. Measurements were calibrated with blank samples that followed national standards (GSR-5, GSR-6, and GSD-9). The relative standard deviation of trace elements was within 2%.

A certain internal relationship exists between the crystal structure and the X-ray diffraction pattern, thus, the X-ray diffraction phenomenon in the crystal is used to obtain the characteristics of the X-ray signal after diffraction. Based on the spectrum information, the object can be determined. This method is the XRD analysis method [33–35]. The instrument used in this study for the XRD is Dutch PANalytical (Empyrean). First, we take 6–10 g of rock sample and coarsely crush it (grain size is less than 1 mm) and then put the ball mill to crush the sample to a particle size further below 44 μm. The scanning range is 5–45° (2θ angle), and the scanning step is 0.02°/min. Finally, we apply the K value method to integrate the various types of diffraction peaks in the XRD pattern to calculate the relative percentage content of various minerals.

A fresh rock sample was polished on both sides to a thickness of 0.03 mm to make a thin rock slice. Zeiss Axio Scope A1 is used for the polarizing microscope thin

Figure 2: Photographs of outcrops in the study area. (a) Panoramic view of the Shanshuihe outcrop. (b) Panoramic view of the Yaoqu outcrop. (c) Yaoqu outcrop, the overlying debris-flow sandstone dragging the underlying muddy-debris-flow sediment.

plate identification. The pores in the cast lamella can be observed through a microscope. The area occupied by the pores in the lamella can be counted and then the ratio of the pore area/total surface area can be estimated.

Hitachi IM4000 argon ion polishing instrument is used for argon ion polishing analysis. We first cut a rock sample into a 1 cm^3 cube, grind the cube in a grinder, and then calibrate under a microscope. After 2–3 h, the polished surface is plated with gold, and the gold-plated sample is placed in a scanning electron microscope sample chamber for analysis. The FESEM method is based on the principle of secondary electron imaging. Based on coated films, we observe samples on the nanometer scale at low voltage to obtain faithful original appearance and ultra-thin topographic structure information on the sample surface [36–38]. ZEISS field emission scanning electron microscope, which was scanned separately through secondary electrons and backscattering, is used in this study for FESEM. The mineral composition was identified by energy spectrum analysis.

4 Results and interpretation

4.1 Internal sedimentary structures of the massive sandstones

4.1.1 Mudstone clasts and intraclast muddy coatings

Many of the samples were collected from mudstone clasts, muddy coatings of the intraclasts within the massive sandstones, associated debris-flow mudstones, and laminated mudstones for trace element geochemical analysis. The discriminating sedimentary environment parameters were used to compare and analyze the genetic relationship among the four different sample types to provide evidence for the origin of the mudstone clasts and muddy coatings.

Natural oxidation–reduction reactions play an important role in controlling migration, symbiosis, and precipitation of vanadium (V), molybdenum (Mo), uranium (U), and other valence-variable elements. These reactions can change the original migration state of the elements so that different valence states or their symbiotic elements are separated, resulting in their redistribution in different environments [39]. For example, U has a low valence (U^{4+}) under reducing conditions and does not dissolve in an aqueous medium, leading to sedimentary enrichment. However, in an oxidizing environment, U shows a high valence (U^{6+}) and easily migrates, resulting in a loss of U in sediments. Thorium (Th) exhibits significant differences from U. Th only has one valence state (Th^{4+}), which is relatively insoluble and generally not affected by redox conditions [40].

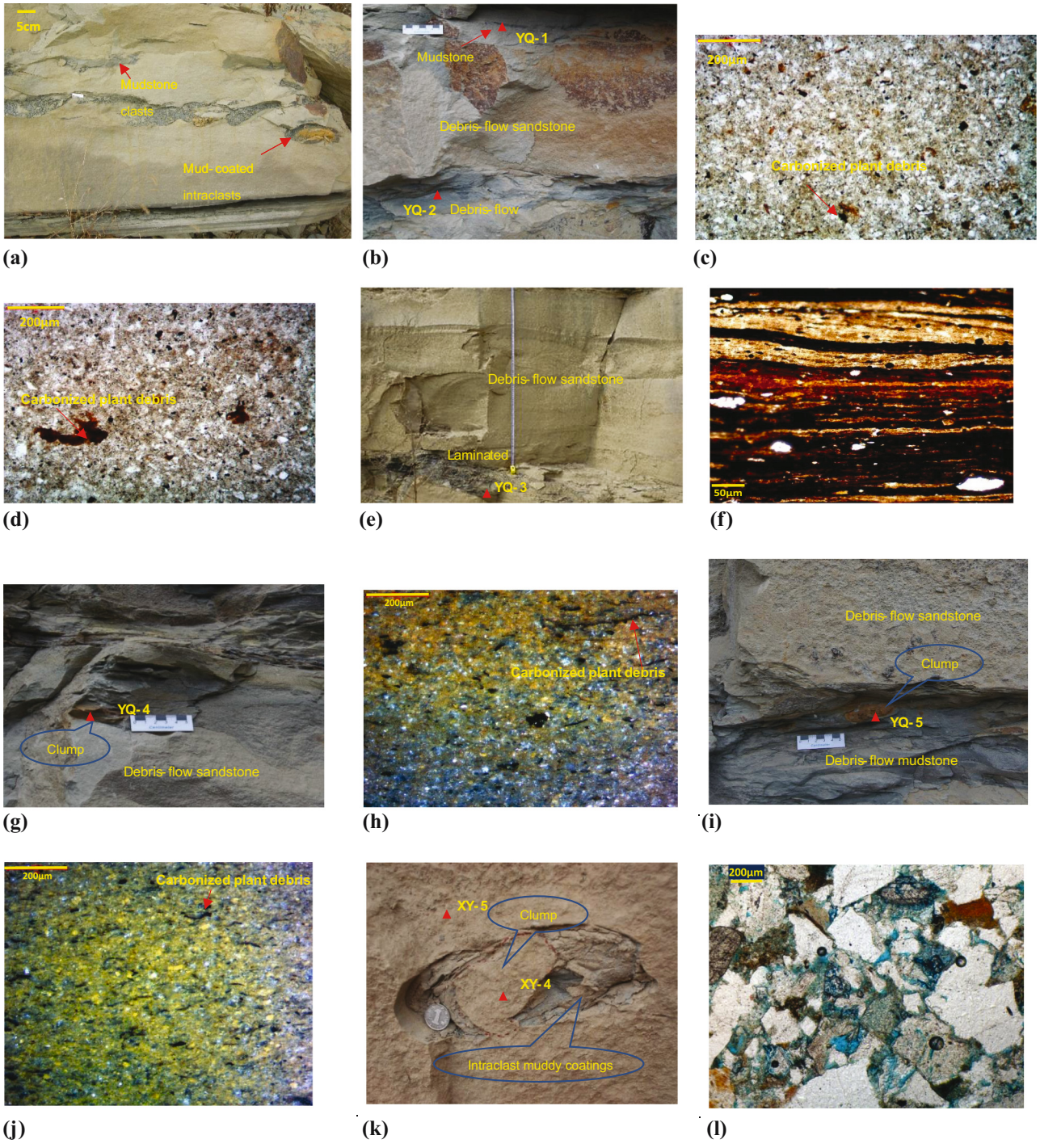

Figure 3: Photographs of the typical sedimentary structures and the thin sections. (a) Yaoqu outcrop: floating mudstone clasts and mud-coated intraclasts in the debris-flow sandstone. (b) Yaoqu outcrop: the mudstone clasts and the debris-flow mudstone. (c) YQ-1: see the position in (b), silty mudstone with a small amount of carbonized plant debris. No directional structure, plain light. (d) YQ-2: see the position in (b). Silty mudstone with a small amount of carbonized plant debris. No directional structure, plain light. (e) Yaoqu outcrop: massive sandstone and associated deep lake–semi deep lake laminated mudstone. (f) YQ-3: see the position in (e). The deep lake–semi deep lake mudstone with the laminated structure, plain light. (g) Yaoqu outcrop: a clump within the debris-flow sandstone. (h) YQ-4: see the positon in (g), silty mudstone with a small amount of carbonized plant debris, reflective optics. (i) Yanqu outcrop: a clump within the debris-flow mudstone. (j) YQ-5: see the positon in (i), silty mudstone with a small amount of carbonized plant debris, slightly directional structure, reflective optics. (k) Shanshuihe outcrop: a mud-coated intraclast within the debris-flow sandstone. (l) XY-4: see the position in (k). Anisometric feldspathic litharenite, plain light.

Besides, diagenesis has little effect on some elements, such as Th and U, and the reactions are still weak before shallow metamorphism. Even with changes in concentrations, the ratios and distribution patterns of related elements remain parallel [41–44]. Therefore, the Th/U ratios are commonly used to judge the redox state of a depositional environment [45,46]. The Th/U ratio value within 2 indicates an anoxic environment. The larger the value, the higher the oxidation level. The Th/U value can even reach 8 under strong oxidation conditions [40]. In addition, the authigenic U content (AU = U_{total} − Th/3) is generally regarded as an important indicator of an ancient anoxic environment. Some researchers determine δU on the basis of the relationship between the AU content and the total U content (δU = $2U_{total}/(U_{total}$ + Th/3)). If δU > 1, it indicates an anoxic environment and if δU < 1, it suggests the oxic environment [47–49].

In this study, the δU and the Th/U data showed two general groups (Figure 4): (1) samples from laminated mudstones of the deep lake-semi deep lake have the Th/U ratio value smaller than 2 and the δU value larger than 1, indicating the anoxic sedimentary environment. (2) Samples from the mudstone clasts, muddy coatings, and debris-flow mudstones exhibited higher Th/U ratios (4–6) and δU < 1, indicating the oxic sedimentary environment. The Th/U ratios and δU from the same outcrop are similar and distinct from the other outcrop.

Vanadium-to-nickel (V/Ni) ratios were used as a bottom water redox state indicator where the values increase as the degree of reduction becomes stronger [40,41]. Some researchers have used the V/Ni ratios to study changes in the reducing ability of a water body

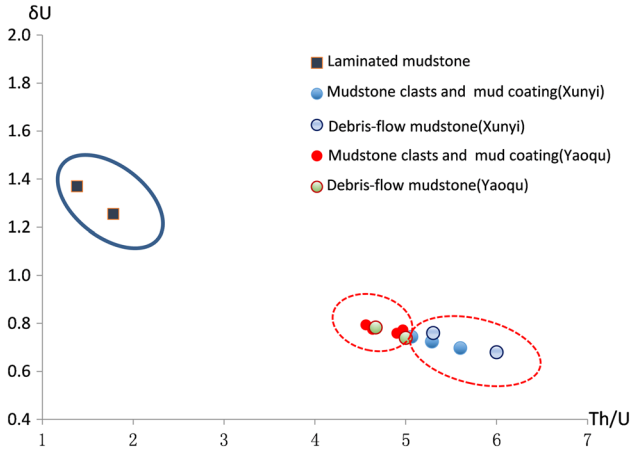

Figure 4: The cross plot of δU and Th/U values of the mudstone clasts, mud coating, laminated mudstone, and debris-flow mudstone.

which was shown during the evolution of the Chang 7 sub-members (7_3, 7_2, and 7_1) [50]. Moreover, the V/(V + Ni) ratios reflect the environmental redox ability [45,51,52]. The high values (>0.84) indicate the stratification of the water body and a strong anaerobic environment containing H_2S in the bottom water. Intermediate values (0.64–0.82) suggest an anaerobic environment with weak stratification, and low values (0.46–0.60) imply a suboxic environment with weakly stratified water [53].

The V/Ni and V/(V + Ni) data also showed two general groupings (Figure 5). The samples from laminated mudstones (V/Ni values of >6 and V/(V + Ni) values of >0.84) reflect a stratified water body with a strong anaerobic environment. In contrast, the samples from mudstone clasts, muddy coatings, and debris-flow mudstones (V/Ni ratios of 1–5 and V/(V + Ni) values of 0.64–0.8) imply an anaerobic water body with weak stratification. All of the sample ratios from the same outcrop were similar and distinct from the other outcrop.

The Th/U, δU, V/Ni, and V/(V + Ni) data resulted in consistent interpretations and similar conclusions. The results indicated that the mudstone clasts and muddy coatings have a strong affinity with the debris-flow mudstones and are quite different from the laminated mudstones. The Yaoqu section showed stronger reduction conditions because it was closer to the center of the paleolake basin (Figure 1b).

Strontium (Sr)-to-barium (Ba) ratios were used to estimate the paleosalinity. The solubility of Ba compounds is lower than that of Sr compounds, and the combination of Ba^{2+} and SO_4^{2-} easily precipitates insoluble $BaSO_4$. Therefore, nearshore sediments are enriched in Ba, and Sr is abundant in deeper water owing to its strong migration ability [45]. Previous studies concluded that the Sr/Ba ratios are generally >1 in saline lake sediments and brackish water and <1 in freshwater sediments. The abundance of Sr in saline water is generally (800–1,000) × 10^{-6}, while in freshwater it is (100–300) × 10^{-6} [45,46].

We found that the Sr/Ba values did not exceed 0.6, and the abundance values of Sr were less than 250 × 10^{-6} (Figure 6), implying that the samples came from a brackish to freshwater environment. The laminated mudstone samples showed the highest Sr/Ba values and Sr abundances (Figure 6), revealing that the samples originated in a water body with a relatively higher salinity. In contrast, samples from the mudstone clasts, muddy coatings, and debris-flow mudstones showed lower Sr/Ba values (generally <0.5) and Sr abundances (less than 200 × 10^{-6}), indicating the water

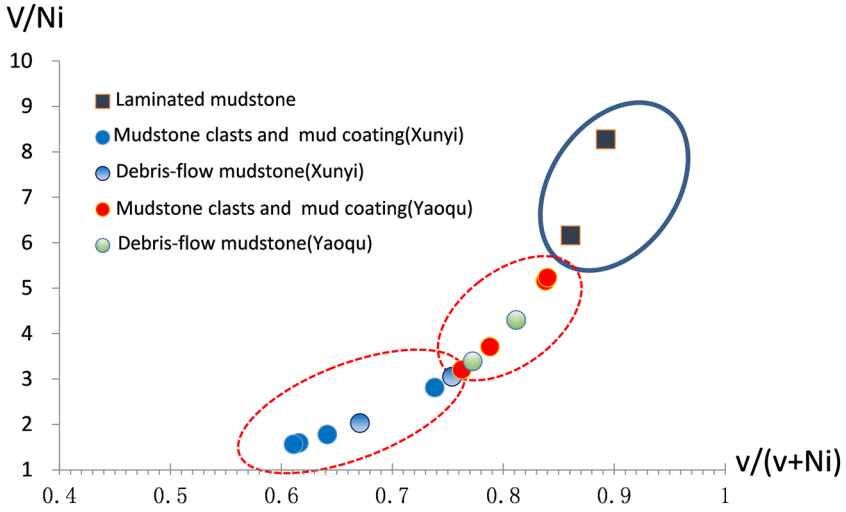

Figure 5: The cross plot of V/Ni and V/(V + Ni) values in mudstone clasts, muddy coatings, laminated mudstone, and debris-flow mudstone.

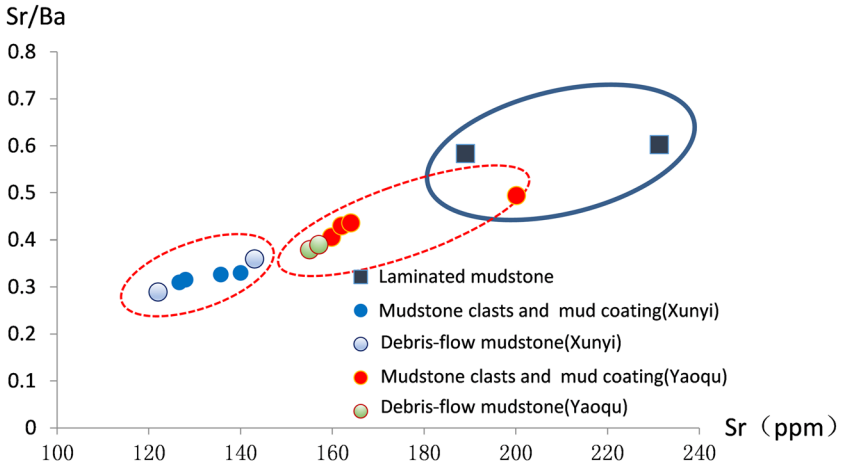

Figure 6: The cross plot of Sr content and Sr/Ba values in mudstone clasts, muddy coatings, laminated mudstone, and debris-flow mudstone.

body with a relatively lower salinity. All of the samples from the same outcrop were similar and distinct from the other outcrop, with Yaoqu showing a slightly higher salinity.

The results indicate that the mudstone clasts, muddy coatings, and debris-flow mudstones were formed under relatively low salinity, which differs from the relatively higher salinity suggested by the laminated mudstones from the deep lake–semi deep lake. Because Yaoqu was closer to the center of the paleolake (Figure 1b), its paleosalinity was slightly higher.

The XRD results showed that the compositions of mudstone clasts and mud coatings were very close to the associated debris-flow mudstones, which contained about 50% clay and relatively high dolomite. However, the composition of laminated mudstones was different, which are mainly composed of clay (>70%) and a small amount of feldspar and quartz without dolomite (Table 1 and Figure 7).

The thin section observations showed that the mudstone clast lithology was predominantly silty mudstone and generally contained a small amount of carbonized plant debris (0.5–6%) and some residual bio-structure (Figure 3c). This demonstrates that the mudstone clasts were formed in a shallow water sedimentary environment, which is consistent with the elemental geochemistry results. The microscopic features of the clasts within debris-flow sandstone were similar to those of the associated debris-flow mudstones (Figure 3c and d).

Table 1: XRD bulk composition analysis of the mudstone clasts, clumps, laminated mudstones, and debris-flow mudstones

Sample no.	Sample type	Content (%)												
		Quartz	K-feldspar	Plagioclase	Calcite	Dolomite	Siderite	Hematite	Analcidite	Barite	Anhydrite	Augite	Ankerite	Clay mineral
XY-1	Mudstone clast	35.8	1.3	1.7		5	1.1			1.7	3.3			50.1
XY-2	Debris-flow mudstone	27	5.3	4		10.5					2.8			50.4
XY-3	Laminated mudstone	17.1	2	4										76.9
YQ-1	Mudstone clast	25	1.2	2.8	6.2	7.4					0.8		7.1	49.5
YQ-2	Debris-flow mudstone	18.3	1.6	10.2	3.2	3.7	0.7		0.4		3.8	3	4.2	50.9
YQ-3	Laminated mudstone	22.1	1	2.8			0.4							73.7
YQ-4	Clump in the sandy-debris-flows	26.4	1.6	5.6	2.5	6.8	2.6	0.8			3.3	4	5.8	40.6
YQ-5	Clump in the muddy-debris-flows	27.1		1.8	9.4		0.6	12.9						48.2

4.1.2 Mudstone clumps and mud-coated intraclast inner cores

The thin section observations and bulk compositions from the XRD analysis suggested that the mudstone clumps and inner cores of the mud-coated intraclasts could be divided into two types: gray-green sandy clumps and yellow-brown muddy clumps (Figure 3a, g, k, and l).

Qiao et al. reported the origin of sandy clumps within the lacustrine mudstones and associated them with paleo-earthquakes [54]. In the interbedded sediments of the delta front, the sand and mud are both water-rich and unconsolidated. The overlying sand, which has a higher density, is pressed into the underlying soft mud to form the bed load structures. Load cast structures were very common in the Yaoqu and Shanshuihe strata from the Chang 7 to Chang 6_3 of Late Triassic age. During the period of deposition of this interval, seismicity was high and seismites frequently developed. Some components of Chang 7 to Chang 6_3 were easy to separate from the parent rocks to form various ball and pillow structures under the action of earthquakes and gravity slides. Zheng et al. found that sandstone spheroids in the Baibao area of the Ordos Basin had fallen into the mudstones of the Chang 6 Member [55], and Li et al. found many sandy ball and pillow structures in drill cores from the Yanchang formation [21]. These results showed that sandy ball and pillow structures generally developed in the Yanchang formation.

Based on the thin section observations, the petrophysical characteristics of the sandy cores of the mud-coated intraclasts were extremely similar to the surrounding rocks (debris-flow sandstone). The lithology was in equigranular feldspathic litharenite (Figure 3l), and their composition and quartz, feldspar, and detrital contents were similar (Table 2). These results indicate that the sandy cores originated from the surrounding or adjacent rock.

A small amount of argillaceous, dolomitic, or iron clumps exists in muddy sediment of shallow lakes or delta fronts, which is a common phenomenon in continental basin sediments [56]. The comprehensive analysis of the argillaceous clumps by using the thin sections and XRD showed that the components and fabric characteristics of the clumps in debris-flow mudstones and massive sandstones were similar (Figures 3h, j, 8 and Table 1). The lithology was slightly oriented silty mudstone with a small amount of carbonized plant debris (Figure 3h and j), which is

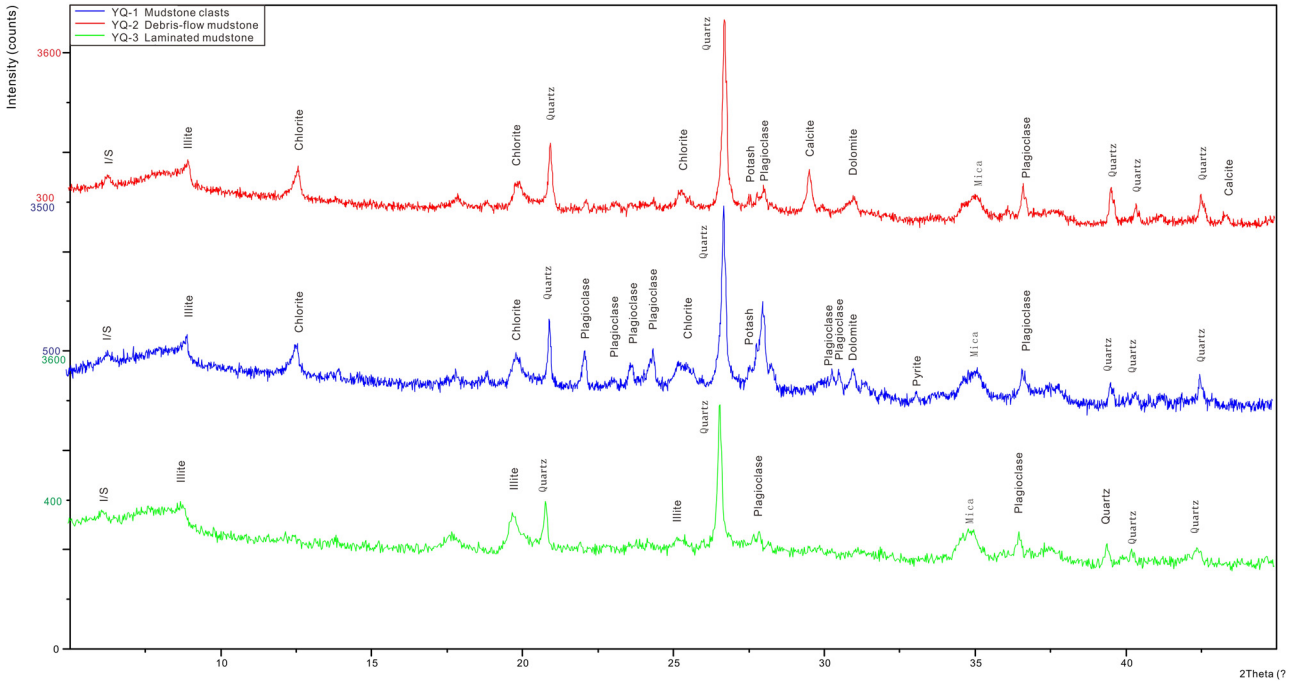

Figure 7: XRD curves of mudstone clasts, the debris-flow mudstone, and the semi-deep lake laminated mudstone.

consistent with the sedimentary characteristics of shallow water environments.

4.2 Genetic mechanism of deep-water massive sandstones

For the origin and genesis of deep-water massive sandstones, previous studies research mostly focused on the observation and description of sedimentary phenomena. The establishment of the genetic model is mainly based on speculation (Figure 9b and c). Shanmugam believes that mudstone clasts are important sedimentary structure developed in a large number of sandstones and has established a deep-water sandstone deposition and transportation model (Figure 9c). However, he did not explain the origin of the mudstone clasts in the debris-flow sandstone. Therefore, his model is not perfect to explain the origin of massive sandstones in deep water. Ito believes that turbidity currents erode the sediments of the underlying bed and can be converted into mudstone clasts-rich debris flows and established a sedimentary evolution model (Figure 9b). However, the experimental data of this study obviously do not support such a deposition model. The trace element parameters indicated that the floating mudstone clasts, clumps, and mud coatings of the intraclasts within deep-water massive sandstones were formed in normal shallow water environments with relatively high oxidation and low paleosalinity. They showed a strong affinity with associated debris-flow mudstones, but not with the associated laminated mudstones (underlying sediment). Furthermore, lithologic compositions showed that the terrigenous clastic and clay mineral contents of the mudstone clasts, clumps, and mud coatings were similar to the associated debris-flow mudstones. In contrast, the clay mineral contents of laminated mudstones were significantly higher.

The clumps and inner cores of the mud-coated intraclasts within the debris-flow sandstone consisted of gray-green sandy clumps and yellow-brown muddy clumps. These clumps were quite developed in the muddy debris-flow sediments associated with the sandstones. Internal clumps of debris-flow sandstones, the whole rock composition and petrological characteristics of the core in the “mud-coated intraclasts” structure are similar to those contained in debris-flow mudstones. We suggest that the massive sandstone provides drag for sliding sediments and the muddy clumps within the muddy debris flows tended to move toward the massive sandstone layers (Figure 2c).

These results show that the mudstone clasts, clumps, and mud-coated intraclasts within debris-flow sandstones originated from the associated debris-flow mudstones not from bed erosion or storm scouring the underlying sediment.

Table 2: Mineralogical composition of the mud-coated intraclast inner cores and surrounding rock

Sample no.	Sample source	Terrigenous component (%)													Particle diameters (mm)	
		Quartz	Feldspar	Pyroclastics	High-grade metamorphic debris	Quartzite	Low-grade metamorphic debris	Dolomite	Mica	Chlorite	Calcite	Ferrodolomite	Silicide	Matrix	Maximum	Main
XY-4	Inner core	38.8	12.8	1.8	1.4	6.2	9.3	4.0	11.0	0.5	0.8	0.6	0.6	12.2	0.50	0.05–0.30
XY-5	Surrounding rock	39.4	15.6	2.4	0.8	5.6	10.0	1.2	10.2	0.8	5.0	0.6	0.0	8.4	0.45	0.06–0.30

The deep water sandstone transportation and deposition process can be divided into the following four stages: the stage of interbedded delta-front sandstone and mudstone (Stage 1), the stage of forming the mass flow complex (Stage 2), the depositional stage of the mass flow complex (Stage 3), and the depositional stage of the turbidite flow (Stage 4) (Figure 9a). In the delta front, rapid deposition drove the slope edge to reach an angle of slope failure. With a trigger from an external force, the soft sediment was then transported to the deeper basin, where the soft mud layer with weak shear resistance in the mass-flow complex was washed into the sand layer that has relatively strong shear resistance. This formed the directionally arranged mudstone clasts (mainly distributed at the top and bottom of a single sand layer), mud-coated intraclasts, and clumps, resulting in the development of the massive sandstones with these special sedimentary structures at the foot of the subaqueous slope or at the bottom of the basin. Formation of the massive sandstones retained the features of mass transport deposition, and sand–mud layers within the soft sediment partly exchanged material and finally formed a lithological mixture under shear stress.

4.3 Significance of exploration

During the formation and evolution of the sandy debris flow, the coarse debris deposits in the delta front of shallow water can be intermittently transported to the deep water. Then, the secondary sedimentation can be performed at the foot of the sedimentary slope and even in the deep lake plain to form the sedimentation between siltstone and mud shale. Polarized light microscopy, argon ion polishing, and FESEM were applied to study the pore development characteristics of silty sandstone and other types of rocks in deep water sedimentary systems due to sandy debris flow. The results show that during the process of moving the sandy muddy soft sediments from the delta front to the deep lake area, although a certain degree of lithological mixing occurs between the sandy and muddy soft sediments under the shear stress effect, this mixing effect is insufficient. The coarse-grained siltstones still have residual intergranular pores and feldspar dissolved pores showing good storage properties. According to scanning electron microscopy (SEM) observations, silty sandstone-derived silty sandstones have micron-sized pores (Figure 10a and b), and the pore radius is mainly distributed between 1 and 8 μm (Figure 11). The sedimentary lithofacies in the semi-deep lake-deep lake

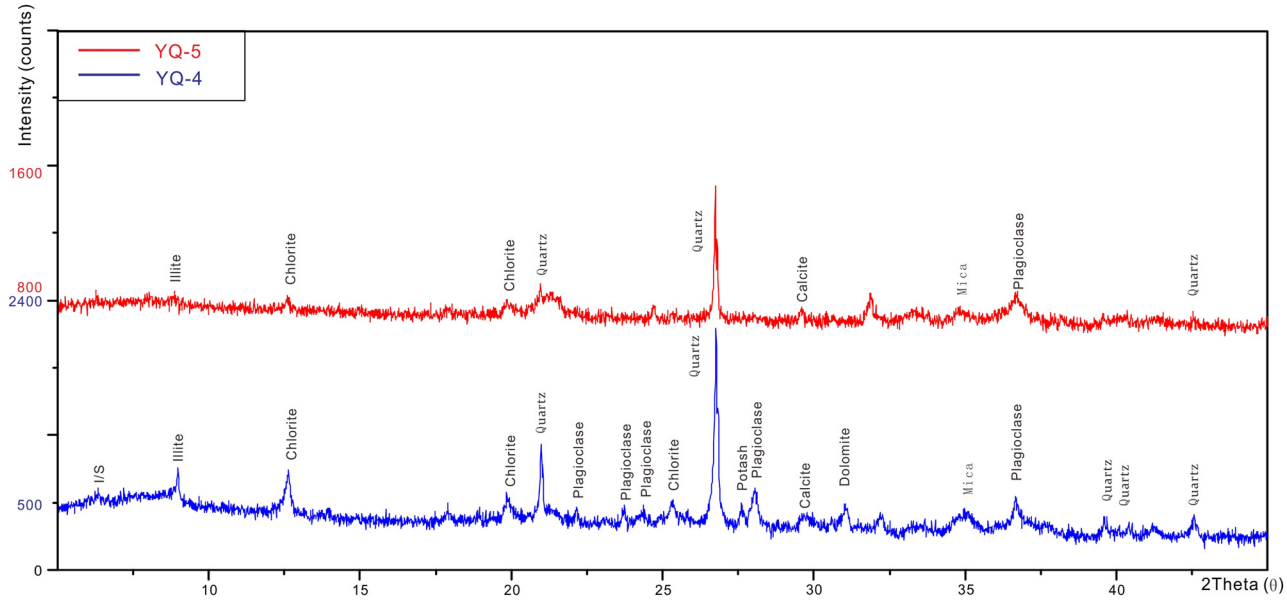

Figure 8: XRD curves of the clumps within the sandy-debris-flows sediment and muddy-debris-flows sediment in Yanqu outcrop.

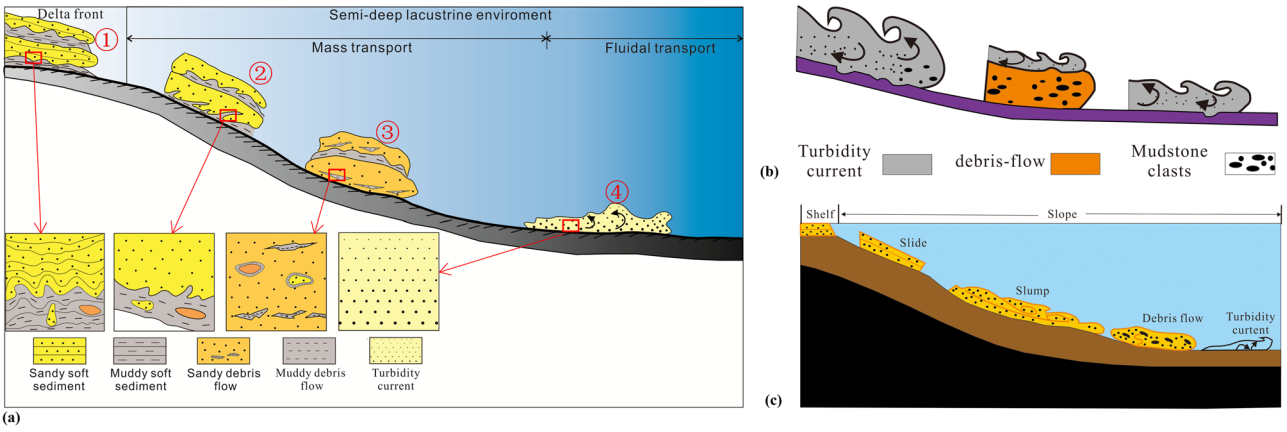

Figure 9: Transport and deposition diagram of deep-water sandstone. (a) The model of this study, (b) the model of Ito, 2008, and (c) the model of Shanmugam, 2013.

only developed a small number of nano-scale pores (Figure 10c and d), and the pore radius was distributed between 20 and 120 nm (Figure 11). Controlled by multiple periods of geological events, debris-flow sandstone of different periods can be stacked on top of each other and interconnected in the horizontal direction. Therefore, the sedimentary thickness is large and the distribution range is wide. Debris-flow sandstone has formed a "sweet spot" reservoir in the deep water sedimentary system. In addition, it is close to the lake basin hydrocarbon generation center, which is conducive to preferential capture of oil and gas. Although the storage performance of this type of reservoir is generally not as good as that of river-delta reservoirs, and the heterogeneous multi-porous medium formed by this kind of reservoir is also relatively complex, with the progress of oil and gas development technology, such as the new progress in porous medium fluid flow [57,58], this kind of oil and gas resource has great exploitation potential and considerable commercial value.

5 Conclusions

1. Based on field geological surveys of two deep-water sedimentary outcrops in the Yanchang formation of the Ordos Basin, X-ray diffraction analysis, elemental

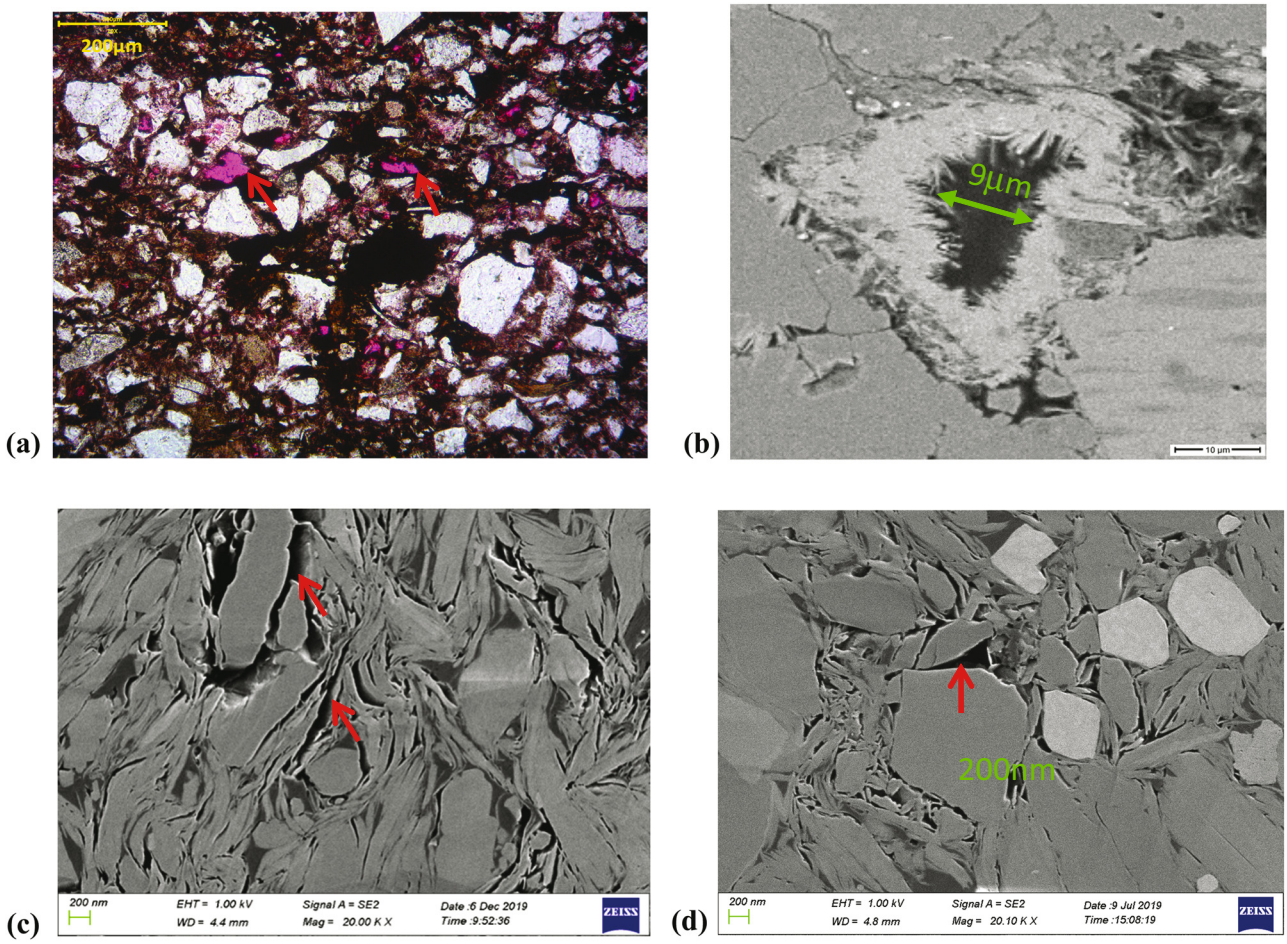

Figure 10: Characteristics of lithological pore development in deep-water sedimentary systems. (a) Debris-flow sandstone. The intergranular residual pores and feldspar dissolved pores are developed. (b) Intergranular residual pores in debris-flow sandstone under FESEM. (c) Siliceous shale. Intergranular pores and intercrystalline pores of clay minerals. The pore size is 20 nm. (d) Siliceous mudstone. Intergranular pores between brittle particles. The pore size is 200 nm.

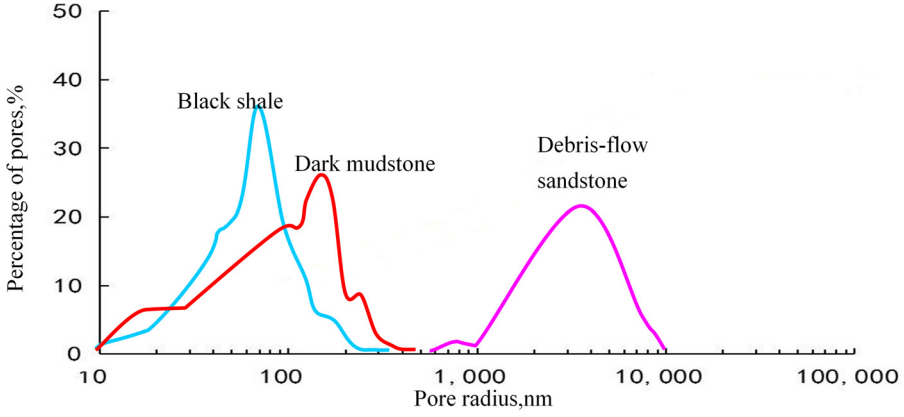

Figure 11: The distribution ratio of pore radii of different lithologies in the deep-water sedimentary system.

geochemical analysis, and polarizing microscope observations were conducted to investigate the causes of various sedimentary structures inside the massive sand bodies from deep-water massive sandstones. The results show that the Th/U values of the mudstone clasts within the massive sandstones and

the mud coatings in the "mud-coated intraclasts" structure are distributed between 4 and 6, and δU <1. The V/Ni values are distributed from 1 to 5 and the V/(V + Ni) values range from 0.64 to 0.84. The Sr/Ba ratio is less than 0.5, and the Sr abundance is less than 200 ppm. The aforementioned parameters indicated a low salinity and partial oxidizing paleowater body. The geochemical characteristics of the sedimentary structure inside the debris-flow sandstone are similar to the associated debris-flow mudstone and completely different from the semi-deep lake facies layered mudstone. Internal clumps of debris-flow sandstones, the whole rock composition, and petrological characteristics of the core in the "mud-coated intraclasts" structure are similar to those contained in debris-flow mudstones. The various sedimentary structures in the debris-flow sandstone are derived from the associated argillaceous debris-flow mudstone, which is not related to the erosion of the underlying lake basin by turbidity, storm erosion, and erosion of underlying sediments.

2. For the origin and genesis of deep-water massive sandstones, previous studies research mostly focused on the observation and description of sedimentary phenomena. The establishment of the genetic model is mainly based on speculation. In this study, through the support of experimental data, the source and evolution of various sedimentary structures such as mudstone clasts and clumps inside the massive sandstones of deep-water sandy debris flow were qualitatively studied, the deterministic model is established. In the delta front slope area, due to the rapid accumulation of sediments, the slope will continue to increase. When the angle of repose is reached, it will cause sandy and muddy soft sediment interbedding to move from the slope area under the effect of gravity to the deep lake plain (the secondary transportation). During the gravity transportation process, the mass transport complex is gradually evolved. The sandy layer with relatively strong shear resistance in the mass transport complex tears the muddy layer with weaker shear resistance and pulls various clumps inside the muddy layer to form deep-water massive sandstones with a special sedimentary structure.
3. Based on the deep understanding of the genetic mechanism of deep-water massive sandstones, the development law of micro–nano reservoir is discussed. Through argon ion polishing and FESEM, the debris-flow sandstones mainly develop micron-scale pores, and the pore radius is mainly distributed in the range of 1–8 μm. The sedimentary rocks from the semi-deep lake to deep lake facies only have a small number of nano-scale pores, and the pore radius is distributed between 20 and 120 nm. The storage performance of debris-flow sandstones is much higher than other rock types. In addition, the sedimentary thickness is large. Therefore, debris-flow sandstones form a "sweet spot" reservoir in the deep-water sedimentary system, which is close to the lake basin hydrocarbon generation center and has huge exploration potential.

Acknowledgments: This work was financially supported by the National Natural Science Foundation of China (No. 41772099) and the National Science and Technology Major Project of China (No. 2017ZX05001-003). The authors would like to thank senior engineers Yuan Xiaoqi and He Jing for their fieldwork participation and assistance with the study. The authors thank Kara Bogus, PhD, from Liwen Bianji, Edanz Editing China (www.liwenbianji.cn/ac), for editing the English text of a draft of this manuscript.

Author contributions: Conceptualization was contributed by J. L. and A. X.; methodology was contributed by J. L. validation was performed by S. L. and X. Z. investigation was performed by J. L. and Z. L.; data curation was contributed by P. Y. and J. D. writing was contributed by J. L. and W. Z.; funding acquisition was contributed by J. L. and R. WY.

Conflicts of interest: The authors declare no conflict of interest regarding the publication of this paper.

References

[1] Bourget J, Zaragosi S, Mulder T, Schneider JL, Garlan T, Van Toer A, et al. Hyperpycnal-fed turbidite lobe architecture and recent sedimentary processes: a case study from the Al Batha turbidite system. Sediment Geol. 2010;229(3):144–59.

[2] Talling PJ, Masson DG, Sumner EJ, Malgesini G. Subaqueou sediment density flows: depositional processes and deposit types. Sedimentology. 2012;59(7):1937–2003.

[3] Valle GD, Gamberi F. Erosional sculpting of the Caprera confined deep-sea fan as a result of distal basin-spilling processes (Eastern Sardinian margin, Tyrrhenian Sea). Mar Geol. 2010;268(1/2/3/4):55–66.

[4] Liang JS, Tian B, Wang Q, Ma XF, Mou WW. Research review, existing problems and future direction of deep-water sedimentary theory. Nat Gas Geosci. 2017;28(10):1488–96.

[5] Shanmugam G. High-density turbidity currents: are they sandy debris flows? J Sediment Res. 1996;66(1):2–10.
[6] Shanmugam G. 50 years of the turbidite paradigm (1950s–1990s) deep-water processes and facies models-a critical perspective. Mar Pet Geol. 2000;17(2):285–342.
[7] Shanmugam G. Deep-marine tidal bottom currents and their reworked sands in modern and ancient submarine canyons. Mar Pet Geol. 2003;20(5):471–91.
[8] Liu F, Zhu XM, Li Y, Xu LM, Niu XB, Zhu SF, et al. Sedimentary characteristics and facies model of gravity flow deposits of late Triassic Yanchang Formation in Southwestern Ordos Basin, NW China. Pet Explor Dev. 2015;42(5):577–88.
[9] Yang RC, He ZL, Qiu GQ, Jin ZJ, Sun DS, Jin XH. Late Triassic gravity flow depositional systems in the southern Ordos Basin. Pet Explor Dev. 2014;41(6):661–70.
[10] Amy LA, Talling PJ. Anatomy of turbidite and debrite sandstones based on long distance (120 × 35 km) bed correlation, Marnoso-arenacea Formation, Northern Apennines, Italy. Sedimentology. 2006;53(1):161–212.
[11] Hodgson DM. Distribution and origin of hybrid beds in sand-rich submarine fans of the Tanqua depocentre, Karoo Basin, South Africa. Mar Pet Geol. 2009;26(10):1940–56.
[12] Middleton GV, Hampton MA. Sediment gravity flows: mechanics of flow and deposition. Turbidites and Deep-water sedimentation. Pacific Section of the Society of Economic Paleontologists and Mineralogists. Short Course Lecture Notes; 1973. p. 1–38.
[13] Shanmugam G. New perspectives on deep-water sandstones: implications. Pet Explor Dev. 2013;40(3):316–24.
[14] Sun NL, Zhong JH, Wang SB, Liu SG, Ni LT, Qu JL, et al. Sedimentary characteristics and petroleum geologic significance of deep-water gravity flow of the Triassic Yanchang Formation in Southern Ordos Basin. J Palaeogeogr. 2017;19(2):299–314.
[15] Hampton MA. The role of subaqueous debris flows in generating turbidity currents. J Sediment Res. 1972;42(4):775–93.
[16] Meng QR, Qu HJ, Hu JM. Triassic deep-marine sedimentation in the western Qinling and Songpan Terrane. Sci China (Ser D): Earth Sci. 2007;37:209–23.
[17] Tang WX, Jiang ZX, Zhang YF. Sedimentary Characteristics and sedimentary model of deep water deposits of late Triassic Chang 7 Member in Southern Ordos Basin. Sci Technol Eng. 2017;17(15):33–41.
[18] Zhou XF, He YH, Wang JG, Li SH, Ling AH. Characteristics of sandy debris flow reservoir from Chang 6 formation in Ordos Basin. Sci Technol Eng. 2014;14(16):216–20.
[19] Ito M. Downfan transformation from turbidity currents to debris flows at a channel-to-lobe transitional zone: the lower Pleistocene Otadai formation, Boso Penisula, Japan. J Sediment Res. 2008;78:668–82.
[20] Ge YZ, Zhong JH, Qu JL, Sun NL, Wang GL. Sedimentary characteristics and storm origin of the sandy debris flow deposits from the Yanchang Formation in the Xunyi region, Ordos Basin: an approach. sedimentary geology and Tethyan. Geology. 2014;34(1):36–46.
[21] Li YH, Liu CY, Wang XJ. Discovery and significance of seismites in late tertiary Yanchang Formation of Ordos Basin. Acta Sedimentol Sin. 2008;26(5):772–9.
[22] Zhang Z, An Y. Nanotechnology for the oil and gas industry–an overview of recent progress. Nanotechnol Rev. 2018;7(4):341–53.
[23] Yang JJ. Structural evolution and petroleum distribution rules in Ordos Basin. Beijing: Petroleum Industry Press; 2002.
[24] He ZX. Evolution and oil-gas in Ordos Basin. Beijing: Petroleum Industry Press; 2003.
[25] Lin HB, Hou MC, Chen HD, Dong GY. Characteristics and evolution of the sedimentary system of upper Triassic Yanchang Formation in Ordos Basin, China. J Chengdu Univ Technol Sci Technol Ed. 2008;35(6):674–80.
[26] Yu J, Han YL, Lin SJ. Geological characteristics and reservoir types of Triassic Yanchang Formation in Ordos Basin. China Petroleum Exploartion. 2001;6(4):13–19.
[27] Li XB, Yang ZL, Wang J, Liu HQ, Chen QL, Wanyan R, et al. Mud-coated intraclasts: a criterion for recognizing sandy mass-transport deposits–deep-lacustrine massive sandstone of the upper Triassic Yanchang Formation, Ordos Basin, Central China. J Asian Earth Sci. 2016;129:98–116.
[28] Zou CN, Wang L, Li Y, Tao SZ, Hou LH. deep-lacustrine transformation of sandy debrites into turbidites, Upper Triassic, Central China. Sediment Geol. 2012;265/266:143–55.
[29] Fu ST, Deng XQ, Pang JL. Characteristics and mechanism of thick sandbody of Yanchang Formation at the centre of Ordos Basin. Acta Sediment Sin. 2010;28(6):1081–9.
[30] Li XB, Fu JH, Chen QL, Liu XY, Liu HQ, Guo YR, et al. The concept of sandy debris flow and its application in the Yanchang Formation deep-water sedimentation of Ordos Basin. Adv Earth Sci. 2011;26(3):286–94.
[31] Li XB, Chen QL, Liu HQ, Wanyan R, Wei LH, Liao JB, et al. Features of sandy debris flows of the Yanchang Formation in the Ordos Basin and its oil and gas exploration significance. Acta Geologica Sin. 2011;85(5):1187–202.
[32] Liao JB, Xi AH, Li ZY, Liu HQ, Li XB, Wanyan R. Microscopic characterization and formation mechanisms of deep-water sandy-debris-flow and turbidity-current sandstones in a lacustrine basin: a case study in the Yanchang Formation of the Ordos Basin, China. Pet Sci. 2018;15:28–40.
[33] Morillas H, García-Galan J, Maguregui M, Marcaida I, García-Florentino C, Carrero JA, et al. Assessment of marine and urban-industrial environments influence on built heritage sandstone using X-ray fluorescence spectroscopy and complementary techniques. Spectrochim Acta, Part B. 2016;123:76–88.
[34] DäHn R, Popov D, Schaub P, Pattison P, Grolimund D, MäDer U, et al. X-ray micro-diffraction studies of heterogeneous interfaces between cementitious materials and geological formations. Phys Chem Earth, Parts A/B/C. 2014;70-71:96–103.
[35] Goyal A, Khatri I, Singh AK, Sharma R, Mohan M. X-ray diffraction patterns and diffracted intensity of kα spectral lines of he-like ions. Radiat Phys Chem. 2017;138:16–21.
[36] Deng H, Hu X, Li HA, Luo B, Wang W. Improved pore-structure characterization in shale formations with FESEM technique. J Nat Gas Sci & Eng. 2016;35:309–19.
[37] Clausell JV, Bastida J, Serrano FJ, Pardo P, Huertas FJ. A new FESEM procedure for assessment of XRD microstructural data of kaolinites. Appl Clay Sci. 2017;37(1–2):127–32.

[38] Nahak S, Chattopadhyaya S, Dewangan S, Hloch S. Wear characterization into Wc-Co by FESEM. Mater Today Proc. 2018;5(2):3533–40.
[39] Tonger, Liu WH, Xu YC. The discussion on anoxic environments and its geochemical identifying indices. Acta Geologica Sin. 2004;22(2):365–72.
[40] Kimura H, Watanabe Y. Ocean anoxia at the Precambrian-Cambrian boundary. Geology. 2001;29:995–8.
[41] Alberdi–Genolet M, Tocco R. Trace metals and organic geochemistry of the machiques member (Aptian-Albian) and La Luna Formation (Cenomanian-Campanian), Venezuela. Chem Geol. 1999;160:19–38.
[42] Liu YF, Qiu ZS, Zhong HY, Nie Z, Li J, Huang WA, et al. Bitumen recovery from crude bitumen samples from halfaya oilfield by single and composite solvents-process, parameters, and mechanism. Materials. 2019;12(17):2656.
[43] Vasconcelos C, McKenzie J, Bernasconi S, Grujic D, Tiens A. Microbial mediation as a possible mechanism for natural dolomite formation at low temperatures. Nature. 1995;377:220–2.
[44] Zhao ZH. The elements of the trace element geochemistry. Beijing: Science Press; 1997.
[45] Deng HW, Qian K. Sedimentary geochemistry and environment analysis. Lanzhou: Gansu Science and Technology Press; 1993.
[46] Jones B, Manning DAC. Comparison of geochemical indices used for the interpretation of palaeoredox conditions in ancient mudstones. Chem Geol. 1994;111:111–29.
[47] Steiner M, Wallis E, Erdtmann BD, Zhao YL, Yang RD. Submarine hydrothermal exhalative ore layers in black shales from South China and associated fossils-insights into a Lower Cambrian facies and bio-evolution. Palaeogeogr Palaeoclimatol Palaeoecol. 2001;169:165–91.
[48] Yu WM, Tang HM. Experimental study on the existence of nano-scale pores and the evolution of organic matter in organic-rich shale. Nanotechnol Rev. 2019;8:156–67.
[49] Wignall PB, Twitchett RJ. Oceanic anoxia and the end Permian mass extinction. Science. 1996;272(5265):1155–8.
[50] Zhang CL, Gao AL, Liu Z, Huang J, Yang YJ, Zhang Y. Study of character on sedimentary water and palaeoclimate for Chang-7 Oil Layer in Ordos Basin. Nat Gas Geosci. 2011;22(4):582–6.
[51] Hatch JR, Leventhal JS. Relationship between inferred redox potential of the depositional environment and geochemistry of the Upper Pennsylvanian (Missourian) Stark Shale. Member of the Dennis Limestone, Wabaunsee County, Kansas, USA. Chem Geol. 1992;99:65–82.
[52] Rimmer SM. Geochemical paleoredox indicators in Devonian-Mississippian black shales, Central Appalachian Basin (USA). Chem Geol. 2004;206:373–91.
[53] Miao JY, Zhou LF, Deng K, Han ZY, Bu ZQ. Relationship between the depositional environment and geochemistry of Permian hydrocarbon source rocks in the Turpan depression. Geol China. 2004;31(4):424–30.
[54] Qiao XF, Guo XP, Li HB, Gou ZH, Su DC, Tang ZM, et al. Soft-sediment deformation in the Late Triassic and the Indosinian Tectonic Movement in Longmenshan. Acta Geologica Sin. 2012;86(1):132–56.
[55] Zheng RC, Wen HG, Han YL, Wang HH, Zheng C, Cai JL. Discovery and significance of sublacustrine slump turbidite fans in Chang-6 oil-bearing formation of Baibao region in Ordos Basin, China. J Chengdu Univ Technol (Nat Sci Ed). 2006;33(6):566–75.
[56] Wang CY, Zhen RC, Gao BY, Zhu GJ, Hu XQ, Li Y. Deep-water fan sedimentary characteristics of Zhujiang Formation in Liwan area of Zhujiang River Mouth Basin. Geol China. 2010;37(6):1628–37.
[57] Gohil VP, Meher R. Effect of magnetic field on imbibition phenomenon in fluid flow through fractured porous media with different porous material. Nonlinear Eng. 2018;8:368–79.
[58] Patel HS, Meher R. Effect of heterogeneity on imbibition phenomena in fluid flow through porous media with different porous materials. Nonlinear Eng. 2018;8:46–65.